Minerals Engineering 177 (2022) 107371

Contents lists available at ScienceDirect

Minerals Engineering

journal homepage: www.elsevier.com/locate/mineng

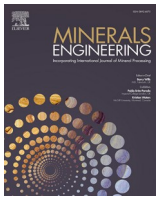

# Investigation of Sensor-Based sorting and selective comminution for pre-concentration of an unusual parisite-rich REE ore, South Namxe, Vietnam

Alan Cardenas-Vera [a], Max Hesse [b,1], Robert Möckel [a,*], R. Gerhard Merker [c], Thomas Heinig [a,2], Quang Van Phan [d]

[a] Helmholtz-Zentrum Dresden-Rossendorf, Helmholtz-Institute Freiberg for Resource Technology, Chemnitzer Str. 40, 09599 Freiberg, Germany
[b] TU Bergakademie Freiberg, Institute of Mineral Processing Machines, Lampadiusstraße 4, D-09599 Freiberg, Germany
[c] Merker Mineral Processing (MMP), Oertenroeder Str. 21, 35329 Gemuenden, Germany
[d] Faculty of Environment, Hanoi University of Mining and Geology, Hanoi 100000, Vietnam

ARTICLE INFO

*Keywords:*
Sensor-Based Sorting
Selective Comminution
Mineral Liberation
X-ray Transmission
Parisite

ABSTRACT

The South Namxe deposit in Vietnam contains unusually high quantities of parisite, in addition to minor quantities of other fluorocarbonates, such as synchysite and bastnaesite. Together these minerals constitute the main REE-bearing minerals. This carbonatite-related deposit presents tabular (dykes) or lens-form ore bodies, up to several tens of meters wide and tens to hundreds of meters in length, that are hosted in Permian limestone and Triassic basalts. The main gangue minerals in the ore bodies are from the barite-celestine solid solution series, ankerite and calcite. It was considered necessary to assess the different grain characteristics presented by the presence of parisite intergrowths and its association with minerals of the barite-celestine solid solution series to structure a probable initial beneficiation strategy. Mineral liberation analysis revealed that an optimal liberation particle size between 45 μm and 90 μm could be achieved without overgrinding the material. Additionally, it showed a strong mineral association between fluorocarbonates, baryto-celestine, and calcite. Grinding below 100 μm is necessary. One substantial energy saving potential is removing the host rock prior to grinding. The potential for pre-concentration with sensor-based sorting and selective comminution is investigated in a pre-study. Sensor-based sorting using X-ray transmission resulted in an enrichment of REE by a factor of 4, a reduction of the mass stream down to approximately 30%, and a loss of rare earths below 2%. Selective comminution using a pin mill, at a circumferential speed of 20 m/s, yielded a recovery of 96.5% of REE minerals and allowed rejection of 27% of barren material. This shows that both selective comminution and sensor-based sorting can be considered as complementary beneficiation steps when processing these REE ores.

## 1. Introduction

The Namxe rare earth element (REE) deposit, located in the Lai Chau province, northwest of Vietnam, is divided into the North Namxe and South Namxe areas by the east–west striking Ban Pan-Phong Tho fault in the Namxe river valley (Nguyen Thi et al., 2014; Phan et al., 2019; Vlasov et al., 1961). Two ore types were identified in the Namxe deposit: a weathered ore in the northern area with a total rare earth oxides (TREO) head grade between 4 and 5 wt% and primary ore in the southern parts showing an average content of TREO of approximately 1.4 wt%. The primary ore consists of parisite, bastnaesite, gadolinite, magnetite, uranopyrochlorite, apatite, barite, and fluorite (Kušnír, 2000; Smith et al., 2016).

This carbonatite-related deposit presents tabular (dykes) or lens-form ore bodies, up to several tens of meters wide and tens to hundreds of meters in length, that are hosted in Permian limestone and Triassic basalts (Nguyen Thi et al., 2014). The TREO resources in the Namxe deposit are approximately 7.7–10.2 million tons (Long et al., 2012; Zhou et al., 2017). There have been several attempts to develop the deposit since 1958; very few undetailed reports of successful

* Corresponding author.
*E-mail address:* r.moeckel@hzdr.de (R. Möckel).
[1] Current address: University of British Columbia, Norman B. Keevil Institute of Mining Engineering, 517-6350 Stores Road, Vancouver, BC Canada, V6T 1Z4.
[2] Current address: Umwelt- und Ingenieurtechnik GmbH Dresden (UIT), Zum Windkanal 21, 01109 Dresden, Germany.

https://doi.org/10.1016/j.mineng.2021.107371
Received 15 December 2020; Received in revised form 29 November 2021; Accepted 21 December 2021
Available online 5 January 2022
0892-6875/© 2022 Elsevier Ltd. All rights reserved.

processing routines are available. The successful mineral processing methods include concentration of REO by gravimetric and magnetic methods and flotation (Dzien, 1990).

Mineralogical studies on the South Namxe ore revealed parisite: Ca $(REE)_2[CO_3]_3(F,OH)_2$ as the main REE-bearing mineral, with minor occurrences of bastnaesite: (REE)$[CO_3]$(F,OH) and synchysite: Ca(REE) $[CO_3]_2$(OH,F) (Heinig et al., 2019). These three minerals are classified as REE fluorocarbonates and contain REE, F, and $CO_3$ ions in the general form of REE $[CO_3]$ F (Owens et al., 2018). Additionally, Heinig et al. (2019) indicated the presence of baryto-celestine that is finely intergrown with parisite on a $<$ 100 μm-scale. The baryto-celestine corresponds to minerals of the barite-celestine solid solution series (Hanor, 2000).

Sensor-based sorting allows rejection of coarse barren particles at an early stage of mineral processing, which results in reduction of input ore and therefore decreased consumption of energy, water, and reagents, in comparison to conventional beneficiation techniques (Lessard et al., 2014). To date, several different sensor technologies for sorting application have been investigated: X-ray fluorescence, X-ray transmission, X-ray luminescence, radiometric, optical, near-infrared spectrometry, Laser (triangulation, induced breakdown spectroscopy, and induced fluorescence), visual spectrometry, and thermal infrared (Lessard et al., 2016; Robben and Wotruba, 2019). However, there is no known commercial use of sensor-based sorting in processing of rare earth minerals (Neubert and Wotruba, 2017; Veras et al., 2020), and prior to Möckel et al. (2019) there is no known reference of beneficiation tests using sensor-based sorting for REE ores with parisite as the main REE-mineral.

In selective comminution, particularly in preferential breakage, barren particles can be rejected during subsequent sieving. The term selective comminution summarizes comminution mechanisms that lead to preferred crack propagation in a particle, which can occur either through a single component or along boundaries between components, e.g., mineral grains. Preferred crack propagation is caused by differences in material properties, which are considered as potential targets for selective comminution. Potential for differences in mineral and rock properties exists within a wide range from mineral grain and coarse particle sizes, and even entire rocks considering selective comminution by blasting. Material properties distinguish different minerals, ore types, and host rock. These properties include mineral grain roughness, hardness, density, toughness, strength, or grindability of the components (Hesse et al., 2017). Exploitation of the potential presented by the above-mentioned differences depends on the comminution system: machines and rock materials; and this potential can be exploited by preferential breakage (preferred crack propagation through a single component), interfacial breakage (preferred crack propagation along boundaries between components or grains), or a combination of the two. Preferential breakage is not a separation method; it transforms material properties, such as strength differences, which are not directly applicable to a sorting process into other material properties (e.g., different contents over size fractions), which represent a separation criterion for a separation process. Preferential breakage results in a more extensive comminution, therefore deriving in an enrichment in the fine fraction and depletion in the coarse fraction of one component. Components that display different comminution behaviors during preferential breakage result in comminution products that display differences in particle-size distributions. For example, the enrichment of ore minerals in finer size fractions after blasting, crushing, or grinding are often the result of preferential breakage. Although preferential breakage is a common phenomenon, it often requires special measures and consideration in order to be economically used in ore beneficiation. Interfacial breakage enhances the degree of liberation for similar-sized or coarser particles compared to random breakage (Hesse, 2018). The South Namxe deposit offers a significant potential pertaining to differences in strengths of host rocks and embedded REE-rich veins and lenses. In this project, we focused on preferential breakage for mass reduction of barren material and developed strategies that would relieve subsequent processes, mainly grinding and flotation.

The dominant presence of parisite as a REE-mineral in the South Namxe deposit, in addition to its close association with baryto-celestine, renders this deposit as unique in terms of its REE ores. The main objective of the South Namxe project was to evaluate application of selective comminution and an on-site sensor-based sorting to the ore to reduce the quantity of non-valuable material that would enter the next processing steps. Additionally, we aimed to investigate a possible beneficiation route for the ore using our test results and previously published results by Möckel et al. (2019) and Merker et al. (2019) on sensor-based sorting and a beneficiation routine. In this study, we use mineral liberation analysis (MLA) to analyze grain sizes, mineral associations, and intergrowths of the main REE-bearing mineral, parisite. This information is then used to structure an optimal beneficiation strategy for the South Namxe ore with emphasis on sensor-based sorting as an initial processing stage.

## 2. Materials and methods

The South Namxe samples correspond to material obtained from drill cores (LK 0512 and LK0709) and outcrops. Drill core material was classified by visual inspection into three rock types: red ore (15.5 kg), yellow host rock (15.5 kg), and green host rock (489 kg). Surface red ore samples (348 kg) were manually collected from outcrops. Each rock type was crushed in a jaw crusher to a particle size of minus 50 mm and subsequently sieved in the facility of the UVR-FIA GmbH in Freiberg, Germany, using 4-, 10-, 16-, and 31.5 mm sieve aperture sizes. The rock types were analyzed with X-Ray Diffraction (XRD), X-Ray Fluorescence (XRF), and Mineral Liberation Analyzer (MLA) to understand mineralogical differences between the four rock types (see Fig. 1):

- Red ore: carbonate-rich rock from drill cores with sharp endings, which indicate and probably represent a dyke or lenses suite. The ore has a distinctive reddish tone, and consists of local granular barite, calcite, ankerite, and minor magnetite. XRD analysis also indicated the presence of parisite, bastnaesite, baryto-celestine, and calcite.
- Yellow host rock (fenite): feldspar-rich, highly calcareous rock, which consists of local quartz veinlets and pyrite. It represents fenitized barren host rock. XRD analysis confirmed the presence of microcline, ankerite, calcite, chlorite, rutile, and albite.
- Green host rock: slightly calcareous volcanic rock with greenish and grayish tones that contains actinolite, albite, epidote, titanite, and minor quantities of biotite identified by XRD analysis .
- Surface red ore: fine-grained carbonate-rich rock found in outcrops or near the surface with a reddish tone, which probably corresponds to the outcropping of the aforementioned red ore. XRD analysis identified bastnaesite, parisite, calcite, and baryto-celestine.

### 2.1. Mineral liberation analysis (MLA)

Material weighing 3.3 kg was obtained after grinding red ore samples in a ball mill ($<$630 μm), followed by subsequent sieving through aperture sizes (μm): 32, 45, 63, 90, 125, 180, 250, 350, 500, and 630. For MLA purposes, selected fractions were merged to form the following final size fractions (μm): $<$ 32, 32–45, 45–63, 63–90, 90–180, and 180–500, and sampled for preparation of grain mounts. In addition, a virtual software-filter was applied to the $<$ 32 μm particle-size fraction dataset to separate the dataset into two new virtual size fractions: $<$10 μm and 10–32 μm. We then created and processed the data set with all the size fractions combined. Subsamples from the final size fractions above, weighing two to three grams, were each mixed with approximately the same volume of graphite, and placed in molds (d = 30 mm) containing epoxy resin to allow formation of hardened blocks. To prevent sedimentation by density-driven segregation and subsequent influence of this process on analysis, the blocks were cut along the vertical

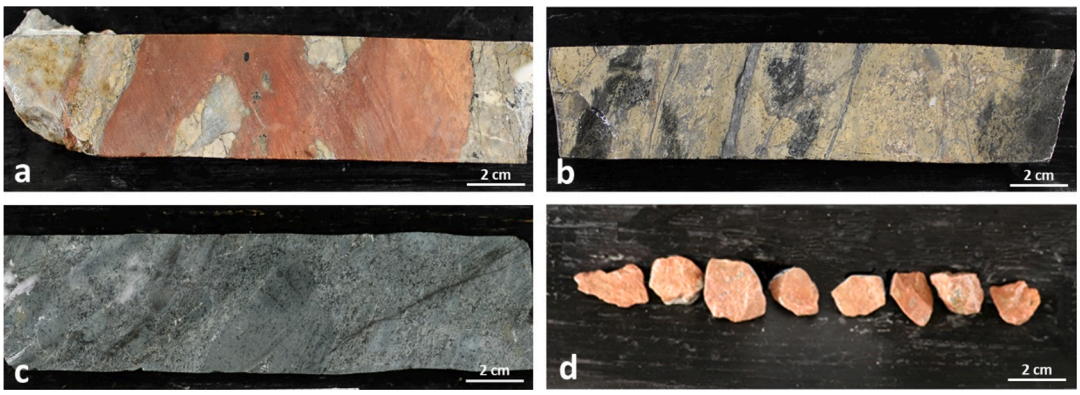


**Fig. 1.** Visually classified rock types from South Namxe. Red ore (a), yellow host rock (b), green host rock (c), and surface red ore (d).

axis, and the new blocks were placed in a new mold with the cut surfaces oriented along the horizontal axis. The blocks were then grinded and polished to expose particles and were later coated with carbon for analysis (Heinig et al., 2015).

All MLA work was performed in laboratories in HIF, Germany. Grain mounts were analyzed using a FEI Quanta 650 FEG scanning electron microscope (SEM) that has two Bruker XFLASH 5010 EDS detectors and a GXMAP measurement mode to perform grid EDX analysis on each detected grain (Fandrich et al., 2007; Bachmann et al., 2017). The SEM was set at a working distance of 12 mm and a horizontal field width (HFW) of 1000 μm with an acceleration voltage of 25 kV and a probe current of 10 μA.

### 2.2. Sensor-Based sorting

Sensor-based sorting technologies (near-infrared spectrometry (NIR), color camera (COLOR), multi-channel Laser (LASER), and X-Ray Transmission (XRT-Density and XRT-Inclusion) were evaluated as options for pre-treating the ore material. The interested reader is referred to Wotruba and Harbeck (2010) and Robben and Wotruba (2019) for a comprehensive description of the principles and technology fundamentals used for sensor-based sorting. Initial experiments were performed on handpicked samples of the size fraction 16–31.5 mm at the facilities of TOMRA Sorting GmbH, Hamburg, Germany.

The sensor-based sorting tests were divided into the following stages:

- **Stage 1.** Pre-Test (first inspection): refers to a fast analysis of ten rock pieces, handpicked from the 16–31.5-mm fraction of the product from the jaw crusher. This was performed for each rock type and a new group of rock pieces denominated “Barren/Carbonates”. The “Barren/Carbonates” group consists of carbonate-rich material that forms the main mass of the carbonatite dykes; it shows a white and/or colorless tone owing to the presence of coarse-grained calcite, ankerite and strontium-rich barite, and locally, magnetite and minor pyrite. The presence of these minerals was confirmed by X-ray diffraction analysis. The “Barren/Carbonates” group was created for calibration and adjustment purposes with an aim to distinguish between REEs and barite before the Bench-Scale Test. The samples were sent to TOMRA to determine which of the different sensors: NIR, COLOR, LASER, and XRT, was most appropriate for sorting the South Namxe ore. This pre-test stage delivers a first qualitative indication as to the suitability of the different set ups of the sensors.
- **Stage 2.** Bench-Scale Test: 107 rock pieces selected from the 16–31.5-mm size fraction of the product of the jaw crusher were sorted using the NIR, COLOR, LASER, and XRT sensors. Chemical analyses (ALS Global, ICP-MS) performed on each of the rock pieces were used to classify the different pieces into waste or ore. The investigation enables correlating between the chemical analyses results of each particle and the sensor-based sorting results (i.e. the basket the particle was sorted into). The content of the TREO of the rock pieces varied between 0% and 16.7%. The cut-off grade for the TREO was set at 0.1%. The TREO value was based on the quantity of each of the rare earth elements (La, Ce, Pr, Nd, Sm, Eu, Gd, Tb, Dy, Ho, Er, Y, Tm, Yb, and Lu). Each of the rock types was evaluated to determine the effectiveness of the individual sensors: 26-rock pieces of red ore, 30-rock pieces of yellow host rock, 26-rock pieces of green host rock, and 25-rock pieces of the surface red ore.
- **Stage 3.** Technical Feasibility Test: this involved using a blend of ore material and host rocks (approximately 33.8 kg), at a ratio of 1:4, for the experiments to mimic a thinning of the carbonate ore by host rock in an open pit mining operation. This ratio was estimated from the geology on site, taking into consideration sizes of veins and their lengths. Results from this test are considered more reliable in terms of technical feasibility, the statistical error of the test is estimated to be as low as 1% (TOMRA, pers. comm.).

### 2.3. Selective comminution

One main objective of this pre-test stage study of the Namxe South ore was to demonstrate occurrence of preferential breakage, a phenomenon that can be used for ore pre-concentration, and to outline a perspective for further investigation with focus on technical applications. The tests were focused on the preferential breakage for different comminution loads between surface red ore and host rock, which had been fully liberated from each other. Liberation and interfacial breakage of rare earth minerals were not analyzed. The South Namxe ore consists of soft REE-containing carbonatite veins and hard host rock. After preferential breakage, the fine size fractions are depleted from the hard host rock and enriched with REE from the soft REE-containing carbonatite veins. The hard host rocks dominants in the coarse size fraction. REE and host rock can further be separated by sieving the comminution products. Success of the separation process depends on REE deportment in size fractions and on the correct choice of sieve aperture. The REE deportment in the size fractions is quantified from mass distribution and content distributions.

The same ratios used in stage 3 of the sensor-based sorting test were used for these tests: a blend of 20% surface red ore and 80% green host rock. Raw materials were pre-comminuted down to $< 5$ mm. Selectivity in the feed material had to be avoided to preserve the material potential for preferential breakage. The capability for preferential breakage of the designated machines can only be investigated if the potential is still in the feed material. Pre-comminution was conducted gently and in a stepwise manner with a roller crusher to achieve as less selectivity as possible in the feed material. The material was fed to the roller crusher several times; the gap size was reduced at each step.

Our choice of comminution devices of laboratory scale was focused to devices that can be scaled-up to satisfy requirements stipulated in the project funding agreement. Nine tests were conducted using three

different laboratory devices: a vertical roller mill (VRM), a pin mill (PM), and a piston die press (PDP). Parameters used in the tests are presented in Table 1. There are more available parameter settings for material and machinery; therefore, we cannot make a general statement about the suitability of these comminution machine for selective comminution.

A VRM test rig simulates the shear free pressure load condition in a VRM. Feed material is crushed in a confined bed. The width of the operating gap is specific to the comminution system and changes according to material properties and the chosen pressure setting. Three different levels of pressure were used.

We used different levels of rotational speed of a PM (RECORD 224 High Performance Universal Mill; Gebr. Jehmlich GmbH). The PM has one pin disk rotor with three rows of pins and one pin disk stator with two rows of pins. The material is fed in the center and moves outwards through the pin rows. Each rotor pin row accelerates the material. The particles impact several times during the path through the pin rows. The diameter of the outer row of pins on the rotor is 219 mm. The PM simulates the impact loading with partly shear loading, similar to those found in several other impact mills.

The PDP (piston diameter of 160 mm) simulates a confined bed load, similar to that found in high-pressure grinding rolls. The material is fed to a die wherein it is compressed by a piston. In this study, three tests were performed at different hydraulic pressures. Calculated hydrostatic pressures of the confined bed are given in Table 1. The holding time at the maximum pressure ($\rho_{max}$) was 2 s for each test.

The particle-size distribution of each comminution product was measured by a minimum of ten size fractions (sieve aperture sequence R 20/3 (ISO 3310–1), ranging from 45 μm to 4 mm and additionally a 32-μm sieve). Chemical analyses were conducted with lithium borate/-metaborate fusion digestion and ICP-OES. Analysis was focused on the main geochemical elements: light REE (+Y), F, Ba, Sr, S, Nb, Th, U, and base metals (Pb, Cu, and Zn).

Particle size is the most frequently used separation criteria in preferential breakage. The aperture size of a sieve behaves as a separation cut and divides a product of preferential breakage into fine and coarse fractions. After preferential breakage, there is additional need for a correct separation cut to achieve a pre-concentrate with high REE recovery and to reject a tailing fraction with negligible losses of REE. For preferential breakage, particle or aperture size behaves as a variable in many evaluation methods, including recovery, enrichment ratio, separation efficiency. Evaluation of preferential breakage using recovery, separation efficiency and grade present a challenge because they depend on the aperture choice for separation of fine and coarse fractions. One integral evaluation method is the SZ Index as it provides a single number to quantify selectivity between barren and valuable material. The SZ index is the difference in selectivity of the feed material ($S_F$) and comminution product ($S_P$) (Hesse et al., 2017; Hesse, 2018).

$$SZ = S_P - S_F$$

The SZ index takes the whole particle size distribution and the whole content distribution into account. The most important advantage of the SZ index is that it allows a simple and fair comparison of preferential breakage of different materials or material properties and different comminution machines or parameter settings of machines (Hesse, 2018). The exploited difference in material properties for the Namxe ore is mainly the strength difference between red surface ore and host rock; investigated differences in comminution machines are the different types of loading and the varied parameter settings. The degree of separation of two components by the particle size is defined by selectivity. Selectivity can be calculated or measured from the area between the cumulative passing curves of both components in a plot whose axis of the linear cumulative passing are in percentage and those of a particle size or aperture size are in logarithm of a length dimension (Hesse, 2018). Feed material can already have selectivity; however, preferential breakage exclusively caused by the investigated comminution machine, and resulting in a change in selectivity of material that begins as feed and terminates as comminution product has to be evaluated. The SZ index quantifies only the change of selectivity. Parameters such as recovery and grade generally cannot be deduced from the SZ index, although they are necessary for a mineral process design. The SZ index does not assess the inherent potential for preferential breakage between the red ore and host rock. Representative samples are used to avoid the necessity to quantify the potential and to consider different potentials in the test evaluation.

A preferred comminution of red ore to fine fraction can cause overgrinding. Pre-concentrate from fine fraction often do not have a sufficient concentration and have to be processed further. An additional constraint was included to minimize the distribution of REE minerals in the fraction $< 5$ μm. The additional constraint was intended to retain the fraction $< 5$ μm below 5% of the mass of the comminution product. It is an outcome of the encompassing flotation investigations at the beginning of this project. The fraction $< 5$ μm showed low selectivity respond at flotation, caused the necessity to remove it prior flotation, and resulted in the consideration as loss due to the lack of concentration opportunities. The content of mass $< 5$ μm will only be documented and evaluated at this early stage of investigating the comminution behavior of the South Namxe ore.

**Table 1**
Selective comminution test parameters.

| Test No. | Test device | Varied parameter (unit) | |
|---|---|---|---|
| 1 | Vertical Roller Mill - test rig (VRM) | Contact Pressure (bar) | 8 |
| 2 | | | 6 |
| 3 | | | 4 |
| 4 | Pin mill (PM) | Circumferential Speed on the outer rotor pin row (m/s) | 50 |
| 5 | | | 30 |
| 6 | | | 20 |
| 7 | Piston Die Press (PDP) | Hydrostatic Pressure $p_{max}$ (bar) | 120 |
| 8 | | | 90 |
| 9 | | | 61 |

## 3. Results and discussion

### 3.1. Mineralogical analysis

Mineral liberation analysis (MLA) were performed to acquire data on modal mineralogy, mineral associations, and mineral liberation for further processing steps. First, we compiled a mineral standard list (library) that contains high quality energy dispersive X-Ray (EDX) spectra for each mineral phase present in the material. Image analysis allowed automatic detection of particle sections by comparing different levels of backscatter brightness. Separated grains were then delineated for EDX analysis to determine the chemistry and therefore define the mineral. This is further supported by investigations using optical microscopy and XRD analyses. It is possible to obtain the modal mineralogy (wt. %) by inferring the volume of minerals based on their density and presence by area in 2-D images (Fandrich et al., 2007). However, it is possible to misidentify minerals. This could occur when corrections are applied, owing to overlapping and interference of X-Ray energy peaks from different REE-bearing minerals. Therefore, caution is advised when applying automated SEM methods to studies of REE minerals (Schulz et al., 2019).

#### 3.1.1. Modal mineralogy

Fig. 2 shows plots of the modal mineralogy of size fractions (μm) $<$ 10, 10–32, 32–45, 45–63, 63–90, 90–180, and 180–500 of the South Namxe ore (red ore from drill cores). In addition, a new particle size class was created and labeled “Combined” to refer to the combination of the different size fractions in proportion to sieve analysis.

There is almost no difference in the concentrations of REE bearing

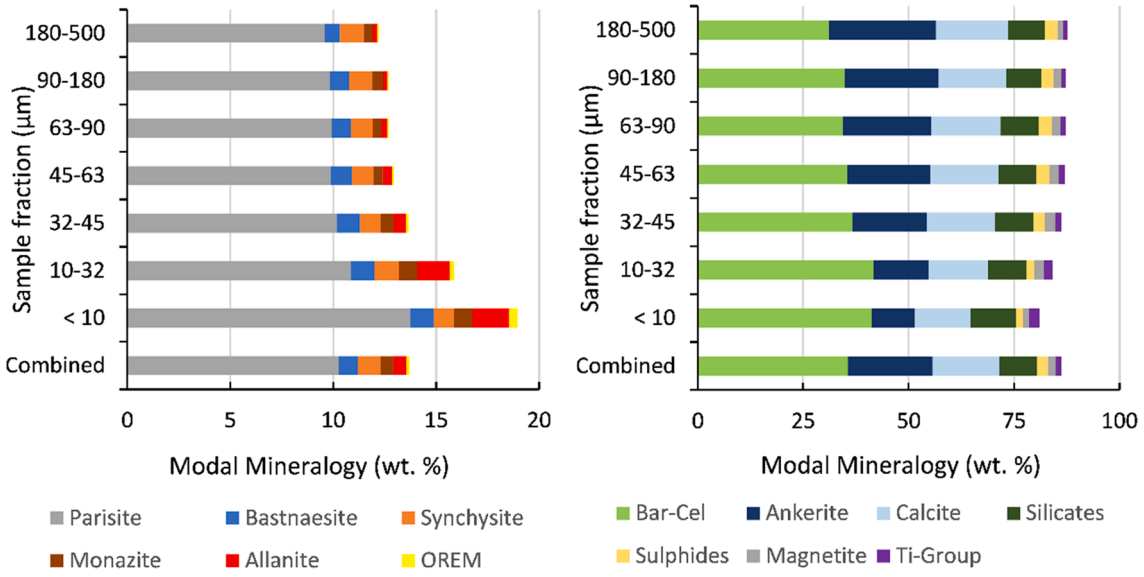


**Fig. 2.** Modal mineralogy for size fractions of samples from South Namxe "red ore" (from drill cores). REE-bearing minerals are on the left and barren minerals are on the right. Each pair of bars from REE minerals and barren minerals for the same size fraction sum up to 100%. OREMs (other rare earth minerals), Bar-Cel (baryto-celestine), and the Ti-Group (ilmenite and rutile).

minerals and barren minerals in the size fractions > 45 µm and < 180 µm. The main rare earth bearing minerals are fluorocarbonates: parisite, bastnaesite, and synchysite, followed by monazite, allanite, and OREMs (other rare earth minerals: gadolinite, huttonite, and samarskite). The content of REE-bearing minerals, particularly parisite and allanite in size fractions that are < 45 µm increases as size fractions decrease.

The baryto-celestine (Bar-Cel) phase represents the main gangue mineral in the red ore. Ankerite and calcite are present in minor quantities. Silicates, magnetite, sulphides (i.e., mainly pyrite and lesser quantities of chalcopyrite, galena, and sphalerite), and the Ti-Group minerals (i.e., ilmenite and rutile) constitute the remaining gangue mineral group. Contents of baryto-celestine and the Ti-Group minerals increase with decreasing size fraction and decreasing total content of gangue minerals. Conversely, ankerite decreases rapidly with decreasing size fraction.

The charts in Fig. 2 show already a distinct selective comminution from grinding the red ore in a ball mill for sample preparation. The feed material consisted of solid drill cores. All particles in the analyzed size fractions < 500 µm were generated by grinding in the ball mill. A random, non-selective size reduction does never cause a change in contents over size fractions. The selective comminution causes a shift of parisite, monazite, and allanite as REE minerals and baryto-celestine and Ti-group minerals into finer size fractions. Ankerite shows distinct remaining in coarser size fraction and depletion in fine size fractions. It is important to note that calcite with a hardness lower than ankerite and quite similar to baryto-celestine does not show distinct enrichment in fine size fractions. The mineral content distribution over size fraction alone does not answer if preferential breakage, interfacial breakage or in which portion both cause the observed shifts in mineral contents. Enrichment of a component in finer size fraction by preferential breakage means above-average frequent breakage events per unit volume in this component. Remaining of a component in coarser size fraction by preferential breakage means below-average frequent breakage events per unit volume in this component. Different contents in size fractions by interfacial breakage presuppose different mineral grain sizes. Interfacial breakage of a coarse-grained mineral will support concentration of this mineral in coarse size fraction equal to the mineral grain size, whereas a fine-grained mineral will be enriched in fine size fractions equal to its grain size. Extensive measurements of the intergrowth between the minerals from samples before and after comminution are necessary to quantify the interfacial breakage.

### 3.1.2. *Mineral association*

It is difficult to achieve complete liberation of minerals; therefore, it is important to evaluate different mineral associations: in this case for rare earth-bearing minerals. Mineral associations refer to the percentage of the length of mineral grain boundaries that are exposed either to the surface (free surface) or in contact with other mineral grains (association). Intergrowths of the same minerals cannot be observed using MLA; thus, they appear as a single grain. Fig. 3 shows the mineral association for parisite in percent per size fraction. A mineral association of a hundred percent corresponds to the sum of the length of all parisite grain boundaries per size fraction.

Parisite grains present high surface exposure for fine fractions of < 10 µm and 10–32 µm, of which the free surface constitutes approximately 99% and 90%, respectively. The minerals phases, bastnaesite and synchysite, constitute the major rare earth-bearing mineral associations of parisite; the remaining contact surface is composed of baryto-celestine and calcite, with a minor presence of ankerite and silicates. Surface exposure for parisite is prominent for size fractions of 32–45 µm and 45–63 µm, of which the free surface constitutes 79% and 68%, respectively.

Bastnaesite and synchysite are the main rare-earth bearing minerals associated with parisite for the same size fractions of 32–45 µm and 45–63 µm; allanite and monazite occur less frequently. For the above-mentioned size fractions, association of parisite with calcite and baryto-celestine seems to be strengthening. Calcite, baryto-celestine, and ankerite are the three minerals mainly associated with parisite in the size fractions of 63–90 µm, 90–180 µm, and 180–500 µm. Synchysite and bastnaesite are the main rare earth-bearing mineral associations followed by allanite and monazite. The free surface of parisite constitutes 55%, 37%, and 20% in the size fractions of 63–90 µm, 90–180 µm, and 180–500 µm, respectively.

In summary, the main target mineral, parisite, is principally associated with baryto-celestine and REE-containing minerals throughout each size fraction. Size reduction by milling leads to a remarkable increase in the free surface of minerals in smaller size fractions; however, there is insignificant change in the overall composition of the associated minerals. This almost equal association in size occurs because of the fine grain size of the minerals and very fine intergrowths with mainly baryto-

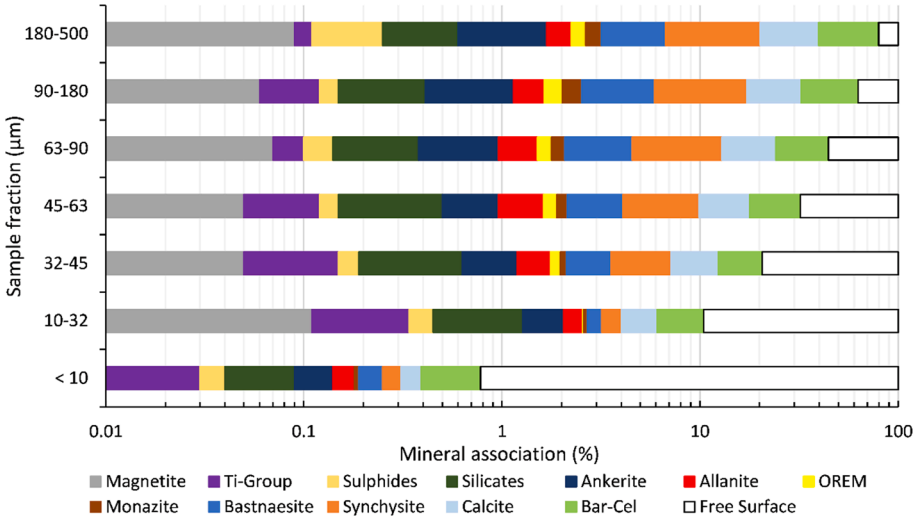


**Fig. 3.** Mineral associations for parisite in the size fractions (µm) < 10, 10–32, 32–45, 45–63, 63–90, 90–180, and 180–500.

celestine. This leads to the conclusion that separation of baryto-celestine from parisite is challenging; neither sensor-based sorting nor milling techniques alone are suitable to address this intimate mineral association. However, concentration through separation of REE minerals from the South Namxe material has been shown to be feasible (Merker et al., 2019; Möckel et al., 2019).

### 3.1.3. *Mineral liberation by free surface*

Exclusively, particles containing parisite are considered for the liberation analysis described below. The liberation analysis is performed on a 2-D section. After grinding, particles contain mineral grains: mostly mineral grain fragments. A particle can consist of a single mineral grain or mineral grain fragment, or a few intergrown mineral grains or mineral grain fragments. Particles that consist entirely only of parisite are considered to be fully liberated parisite particles (100% liberation). Particles containing parisite grains but without any portion of parisite on the particle boundary count fully locked (0% liberation). Consequently, particles consisting partly of parisite and contain parisite on the particle boundary are considered partially liberated.

For this study, liberation "x" is the percentage of the boundary of parisite from a particle that is simultaneously the boundary of this particle. Liberation classes (%) of $\times \leq 40$, $40 < x \leq 60$, $60 < x \leq 80$, $80 < x < 100$, and $\times = 100$, were created to achieve a simple quantification of the liberated parisite boundary that is also exposed to the particle surface. A liberation class of $\times = 100\%$ indicates total exposure or "full liberation" of parisite, whereas a liberation class of $\times \leq 40\%$ indicates that less than forty percent of the boundary of parisite is exposed to the particle surface. Nonetheless, caution is advised as the MLA analysis corresponds to 2-D analysis of surfaces in automated SEM: a particle that is measured as fully liberated in a 2-D section can reveal an intergrowth in the third dimension. That is, 2-D liberation analysis overestimates the real liberation of 3-D particles. No correction was applied in this case.

Fig. 4 provides a summary of liberation of parisite by free surface analysis. The horizontal axis shows the liberation class distribution for all the size fractions. Full liberation was achieved for approximately 97% and 70% of parisite in the size fractions of < 10 µm and 10–32 µm, respectively. This is an indication that parisite is a fine-grained mineral. In contrast, in the coarser fractions of 90–180 µm and 180–500 µm, fully liberated parisite decreases to 4% and 2%, respectively. For the fractions 32–45 µm, 45–63 µm, and 63–90 µm, full liberation is achieved for 48%, 30%, and 16% of parisite, respectively. The quantity of fully liberated particles of parisite rapidly increase with decreasing size fraction. The portion of liberation classes $80\% < x < 100\%$ and $60\% < x < 80\%$ reach the maximum quantities in the fractions 63–90 µm and 90–180 µm and decrease with the increasing portion of fully liberated parisite particles.

Modal analysis of the size fractions, 32–45 µm (R2), 45–63 µm (R3),

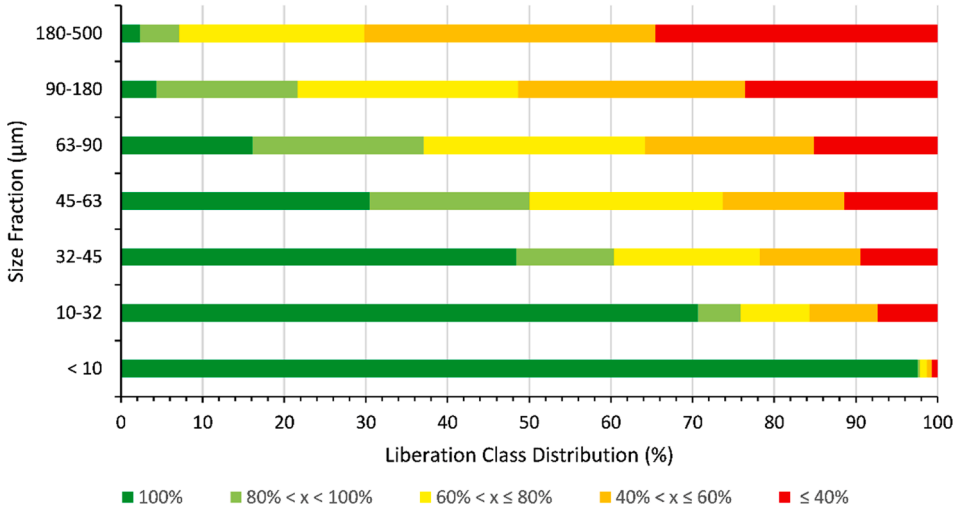


**Fig. 4.** Liberation classes by free Surface of Parisite.

and 63–90 μm (R4) (Fig. 5), indicates that mineral liberation of parisite within the defined liberation classes mostly remains unaltered. Synchysite and bastnaesite remain the major rare earth-bearing minerals accompanying parisite in the three above-mentioned fractions. The presence of allanite and gadolinite increases slightly in the different liberation classes as the size fraction decreases. Baryto-celestine and calcite are the major gangue minerals in the different size fractions.

### 3.2. Sensor-Based sorting (SBS)

In stage 1, ten particles of each rock type occurring in the South Namxe deposit, including the additional "Barren/Carbonate" variety, were exposed to NIR, COLOR, LASER, and XRT sensors to evaluate their suitability for qualified sorting. All sensors were tested in stages 1 and 2, and XRT displayed a superior differentiation of the classes, particularly between the host rock and ore containing REE material. Resulting images of the XRT test in stage 1 are shown in Fig. 6.

In Fig. 6, in the single energy mode, raw XRT images are located to the left, and classified XRT images are located to the right. The black color indicates the presence of dense constituents, i.e., rare earth minerals and baryto-celestine. These results confirm XRF, and chemical analyses results for the red and surface red ores. The yellow host rock displays areas with high absorption that might be the result of the presence of Sr in ankerite or other high dense minerals, such as titanite. The barren/carbonates group presents significant absorption areas (black color) owing to the presence of Sr, W, and Sr-rich barite, as indicated by XRF and chemical analyses. The atomic number of Ba (56) approximates those of La (57), Ce (58), and Nd (60), and this would result in misidentification of minerals as the sensors were calibrated, and the parameters were adjusted. The green host rock presents low absorption (white color), which indicates the presence of light constituents that do not contain rare earth elements. This sharp contrast between the results of ore and gangue material, derived from differences in the average atomic weight, is utilized by the XRT sensor to pre-sort the sample material.

In Fig. 6, in the dual energy mode, raw XRT images are located to the left, and classified XRT images (Background: grey pixels; low atomic density: red pixels; higher atomic density: blue pixels; REEs and baryto-celestine: black pixels) are located to the right. Dual X-ray analysis allows off-setting of the effect of particle thickness and reduction of uncertainty in characterization, which results in more detailed information on X-ray attenuation characteristics. Coloring of the greyscale images would therefore be based on the atomic weight of the particles. However, Ba, La, and Ce have similar atomic weights, as such, classification of REEs, baryto-celestine, and barite as either waste or product is challenging. Therefore, the sensor was further calibrated and adjusted to achieve better classification of the material before conducting performance or feasibility tests.

Hundred and seven rock pieces were selected to conduct the Bench-Scale test in stage 2. Fig. 7 summarizes sorting results using the COLOR, LASER, XRT, and NIR sensors on the rock samples based on a 0.1% TREO cut-off to test for amenability and allocation of different products. XRT-Density and XRT-Inclusions refer to different image processing methods for the raw XRT images.

COLOR sensor results indicated the following probabilities: 54% that product samples terminate in the product class, 46% that product samples are classified as waste. The probability of waste samples being classified as waste was 94%. Classification based on the response of the LASER sensor yielded probabilities of 79% and 86% for product-to-product and for waste-to-waste allocations, respectively. Results of the NIR response of the material were discouraging: a probability of 84% allocation for waste-to-product and 16% for waste-to-waste. XRT-Inclusion sorting achieved the best results. This test yielded a probability of 88% for product-to-product allocation (ore material classified correctly) and a probability of 90% for waste-to-waste allocation (correctly classified waste) for a 0.1% TREO cut-off. Misallocation is restricted to probabilities of 10% for waste-to-product and 12% for product-to-waste. XRT-Density sorting showed a higher probability in waste-to-waste allocation (96%) and a lower probability in product-to-product allocation (81%). This test has limited statistical significance; however, it provides a first impression on capabilities of the different sensors. This is not representative of future production in a mine; however, we aim to define or exclude potential sensors for further larger-scale testing. Additionally, using sensors in combinations could be possible; however, this line of thought was not tested in this study. Initial results of the XRT sensors are promising; and could be reconsidered in the future.

In stage 3 (Technical Feasibility Test), 33.8 kg of material (ore mix of

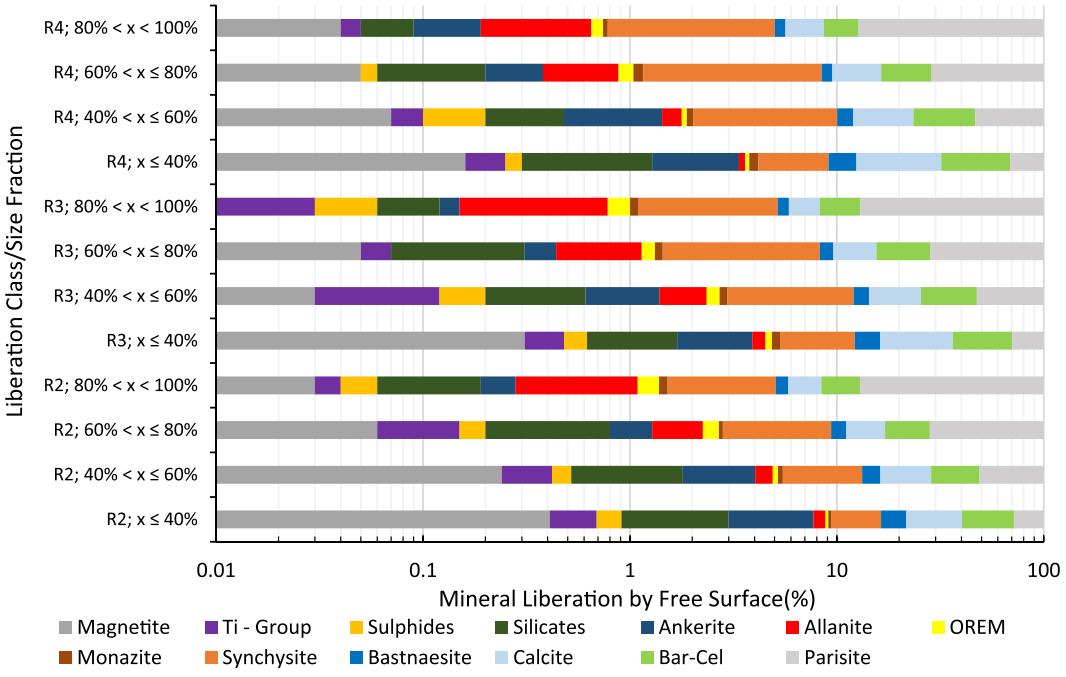


**Fig. 5.** Mineral liberation by free surface for parisite in the fractions R2: 32–45 μm, R3: 45–63 μm, and R4: 63–90 μm.

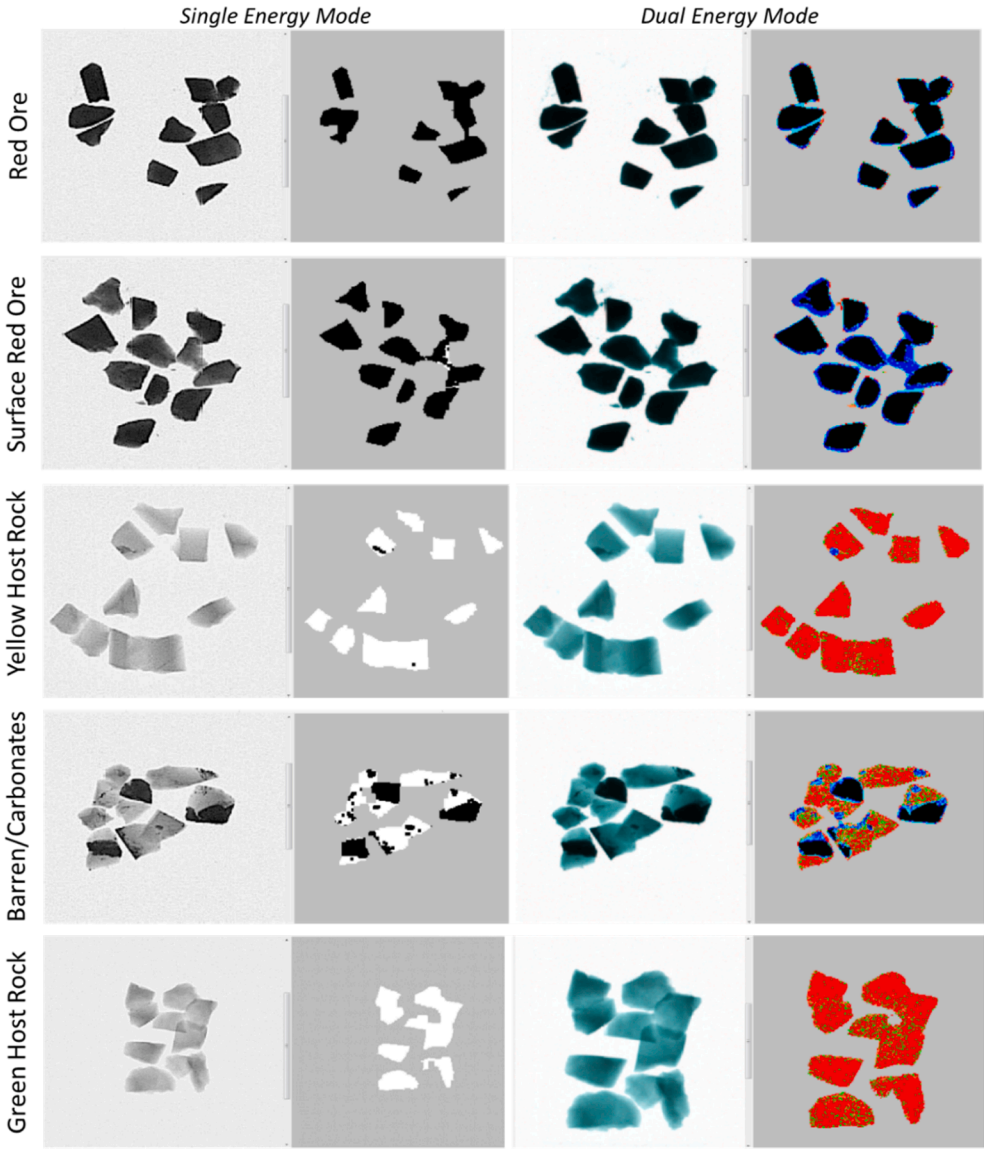


**Fig. 6.** Raw and classified XRT images of the rock classes in the single energy mode and dual energy mode.

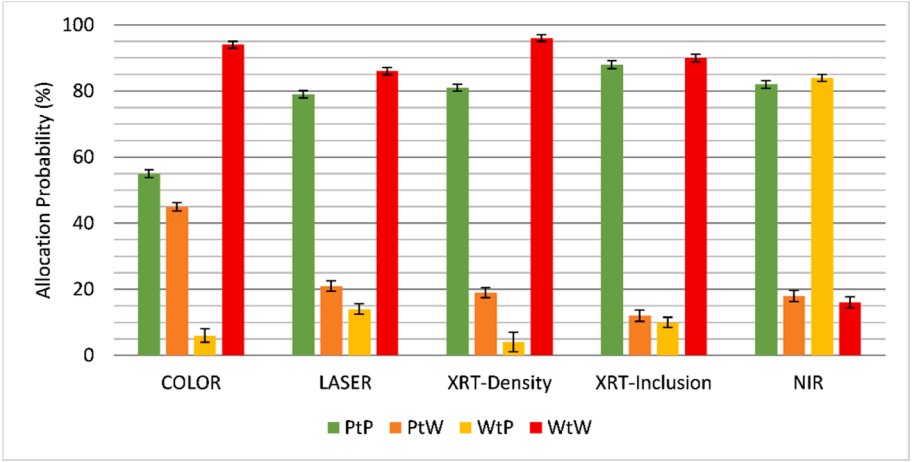


**Fig. 7.** Allocation probability for a 0.1% TREO cut-off for the different sensors evaluated on the South Namxe material. PtP: product to product; WtP: waste to product; PtW: product to waste; WtW: waste to waste.

80% barren host rock and 20% surface red ore, intended to mimic a thinning of the carbonate ore by host rock in an open pit mining operation) from the fraction of 10–30 mm with a head grade of approximately 2.7% LREO (Light Rare earth Oxides – (used as a proxy for TREO in this case), were subjected to a test using XRT-Inclusions configuration sensors. Selection of the sensor for the Technical Feasibility Test was based on results obtained in tests in stage 2, to evaluate the transferability of the previous tests to a large-scale industrial sorting equipment. Results indicated that almost all the material from the host rock and barren dyke were classified as waste, which suggests high separation efficiency of the REE-free silicates (i.e., the host rock) from the REE-bearing particles. The waste fraction contains < 0.1% LREO. Recovery of LREO is 98.4% and grade of the concentrate product is 9.95% LREO. This indicates an increase in the concentration of rare earth elements by a factor of approximately four. These preliminary results indicate a possibility to reduce the mass stream (of a suited particle size) to approximately 30% in an early stage of processing. The loss of rare earths in the tailings was estimated to be below 2%. Not only did these tests confirm the results from stage 2, but they also improved them. Nonetheless, confirmation using scaled-up tests of stage-wise crushing and subsequent sensor-based sorting is needed to determine the maximum proportion possible from sensor-based sorting suited to size fractions. The quantity and content of the produced fine fraction were not quantified in this investigation.

### 3.3. Selective comminution

All tests show a distinct comminution. The comminution ratio of each test approximates two or greater than two. The comminution ratio is calculated using the interpolated sieve aperture sizes at 50% cumulative passing from the feed material and the comminution products (therefore F50/P50 $\geq$ 2). This is the definition of comminution ratio henceforth. Particle-size distributions of all tests are given in Fig. 8; the three tests performed using a VRM test rig produced similar results of particle-size distribution. The comminution degree remains constant for tests conducted at pressures above 4-bars. This is an indication that comminution saturation is reached. For the ore and feed particle size in this project, a dependence relationship between pressure and comminution degree can be expected at lower pressures. The additional constraint requiring that particles smaller than 5 μm be less than 5% mass of the comminution product will be fulfilled. All three samples produce between 5% and 6% of comminuted material at 32 μm. The particle-size distribution is notably similar; therefore, only the sample comminuted at 6-bars is used for the chemical analysis. It can be expected that the comminution products of the other two tests (at 4 bars and 8 bars) show a very similar element distribution.

Comminution performed at 61 MPa and 90 MPa in the PDP resulted in products with similar particle-size distributions. Comminution conducted at 120 MPa resulted in the finest product. Particle-size distributions of the comminuted samples show fluctuations in their relative position compared to a homogeneous material that hardly agglomerates. Properties of these materials are barely known; therefore, researchers currently rely on estimated representativity of material properties. Larger sample mass and more testing cycles at the same parameter settings were required to obtain a continuous shift of the particle-size distribution curves with increasing pressure. The sieved fractions were deagglomerated. Hence, the constraint requiring that particles smaller than 5 μm be less than 5% mass of the comminution product will be fulfilled. The comminution test conducted at a pressure of 120 MPa produced 7% mass smaller than the 32-μm fraction. The other two comminution products resulted in less than 5% mass at the 32-μm size. Finally, two products resulting from comminution at pressures of 90 MPa and 120 MPa were chosen for the chemical analysis.

Tests conducted in the PM resulted in the finest comminution products. Comminution ratios are 4, 12, and 32 for tests conducted at 20 m/s, 30 m/s, and 50 m/s. Therefore, the additional constraint requiring that particles smaller than 5 μm be<5% of the mass of the comminution product will be fulfilled for samples comminuted at 20 m/s and 30 m/s. The comminution at 50 m/s seems to fail this constraint if the particle size distribution is extrapolated. The REE content distributions of all three samples were analyzed afterwards.

Size fractions were analyzed separately for each selected comminution product. The feed material is represented by eight size fractions. The fine fractions contain adequate material to produce a representative (>95% confidence level) sample for chemical analyses. Coarse fractions that resulted in materials inadequate to produce a representative sample were merged to reach the required minimum sample mass for a confidence probability of a minimum of 80%. Eight important elements (La, Ce, Nd, Pr, Th, Y, Ca, and F) are discussed in this article to limit the results section. The evaluation starts with statistic and correlation analysis to determine possibilities for further simplifications. The size fractions show significant differences in the REE content depending on the comminution process and size fraction (Fig. 12). The minimum, maximum, mean values, and the variation coefficient (var.-coeff.) for each analyzed element are given in Table 2. The Table 2 considers all 6 analyzed comminution products. The content values are given as mass percentages and thorium is included because it partly substitutes REE in fluorocarbonates (Nguyen Thi, 2013). SEM data show that approximately 70% of thorium is bonded to fluorocarbonates. Y is a dominant element in gadolinite and samarskite, and it is bonded to

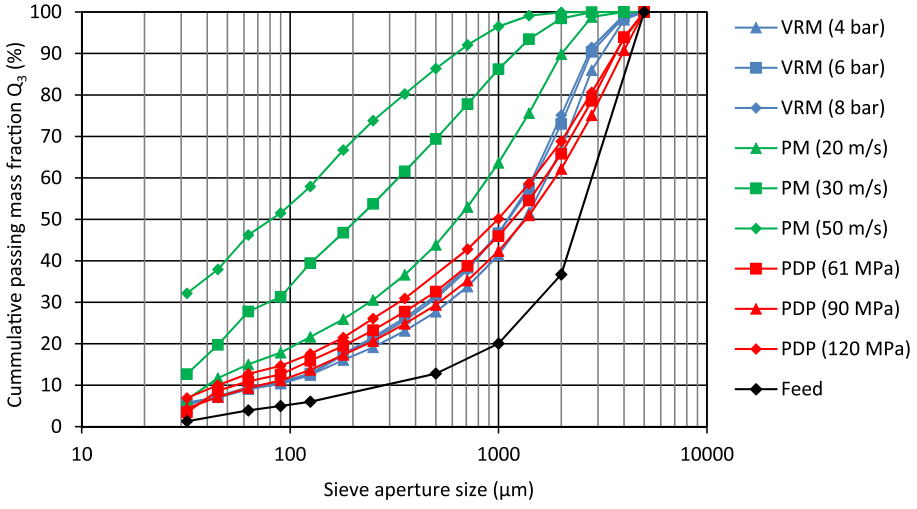


**Fig. 8.** Particle-size distribution of the selective comminution tests. VRM test rig (contact pressure), PM (circumferential speed), PDP (hydrostatic pressure).

**Table 2**
Statistic parameters (in percent unless otherwise noted) of the REE content of all size fractions of analyzed comminution products (Min. – Minimum; Max. – Maximum; var.-coeff. - variation coefficient; b.d.l – below detection limit).

| Element | Min. | Max. | Mean value | var.-coeff. | Coefficient of determination $r^2$ [-] | | | | | | | |
|---|---|---|---|---|---|---|---|---|---|---|---|---|
| | | | | | $CeO_2$ | $Pr_2O_3$ | $Nd_2O_3$ | $Y_2O_3$ | TREO | $ThO_2$ | F | CaO |
| $La_2O_3$ | 0.10 | 4.14 | 2.91 | 40.98 | 1 | 0.71 | 0.93 | 0.90 | 1 | 0.97 | 0.81 | 0.36 |
| $CeO_2$ | 0.18 | 7.06 | 4.83 | 43.19 | | 0.69 | 0.92 | 0.90 | 1 | 0.97 | 0.81 | 0.37 |
| $Pr_2O_3$ | b.d.l | 0.37 | 0.23 | 48.07 | | | 0.82 | 0.72 | 0.73 | 0.65 | 0.67 | 0.05 |
| $Nd_2O_3$ | b.d.l | 1.40 | 0.90 | 41.89 | | | | 0.9 | 0.95 | 0.89 | 0.85 | 0.17 |
| $Y_2O_3$ | b.d.l | 0.06 | 0.04 | 39.01 | | | | | 0.91 | 0.86 | 0.74 | 0.20 |
| TREO | 0.26 | 10.60 | 7.40 | 34.77 | | | | | | 0.97 | 0.83 | 0.33 |
| $ThO_2$ | 0.01 | 0.32 | 0.21 | 37.25 | | | | | | | 0.80 | 0.41 |
| F | 0.16 | 1.17 | 0.77 | 29.85 | | | | | | | | 0.18 |
| CaO | 10.65 | 21.97 | 15.80 | 20.73 | | | | | | | | |

fluorocarbonates and allanite. However, its content is too low for a reliable evaluation of its distribution using the chosen analytical methods. Ca and F (given in Table 2) are both main components in rare earth fluorocarbonates. Correlation strengths between REO, $Y_2O_3$, $ThO_2$, CaO, and F are given in Table 2, with the coefficient of determination ($r^2$). Correlation between $La_2O_3$, $CeO_2$, and $ThO_2$ is strong and yields values between 0.97 and 1. Exclusive of CaO, the lowest correlation values (varying between 0.65 and 0.82) were calculated for $Pr_2O_3$. Coefficients of determination for $Nd_2O_3$ and $Y_2O_3$ are within the ranges of 0.82–0.93 and 0.72–0.9, respectively. Correlation values are 0.67 for fluorine and $Pr_2O_3$; in the range of 0.80–0.81 for fluorine and $La_2O_3$, $CeO_2$ and $ThO_2$; and 0.85 between fluorine and $Nd_2O_3$. The coefficient of determination for correlations between CaO and each of the other elements is low; its values are 0.05 with $Pr_2O_3$ and 0.41 with $ThO_2$.

A more detailed discussion of the outcomes in Table 2 and correlation diagrams is provided below. Correlations of $La_2O_3$-$CeO_2$ and $La_2O_3$-$Nd_2O_3$ are shown in Fig. 9. Chemical analyses were conducted on six comminution products and for all size fractions. There is a strong correlation between $La_2O_3$ and $CeO_2$ (each has a high $r^2$); therefore, it is assumed that the compounds belong either to the same mineral or to different minerals that behave equally during comminution. This indicates absence of selectivity of these compounds to each other, although selectivity can occur in relation to other components. Other correlations, such as $La_2O_3$-$Nd_2O_3$ (Fig. 9b), show higher scattering, which could be attributed to that the lower values are proximal to the detection limit and yield a higher statistic error in the measurement.

The ratios of $La_2O_3/ThO_2$ and $La_2O_3/Y_2O_3$ are plotted in Fig. 10 for each chemically analyzed comminution product and each single size fraction. The majority of ratios of $La_2O_3/ThO_2$ are in the range of 12–16 and those of $La_2O_3/Y_2O_3$ are predominantly in the range 50–80. Ratios of $La_2O_3/ThO_2$ and $La_2O_3/Y_2O_3$ show an influence from the size fraction of samples comminuted in the PM. The ratio of $La_2O_3/ThO_2$ decreases starting from 100 μm for the test at 50 m/s and from 500 μm to bigger size fractions for tests conducted at 20 m/s and 30 m/s. The ratio of $La_2O_3/Y_2O_3$ decreases starting from 100 μm for the test at 50 m/s and from 500 μm to bigger size fractions for tests conducted at 20 m/s and 30 m/s. $La_2O_3$, $Y_2O_3$, and $ThO_2$ are all depleted in the coarse fraction; depletion of the $La_2O_3$ content with increasing size fraction occurs at a faster rate than that of $Y_2O_3$ and $ThO_2$. This is attributed to the different mineralogy of $La_2O_3$, $Y_2O_3$, and $ThO_2$. $La_2O_3$ occurs in abundance in parisite, bastnaesite, synchysite, monazite, and allanite. Yttrium, which partly substitutes REE in fluorocarbonates, is a dominant element in samarskite and gadolinite, and substitutes REE in allanite. Thorium substitutes REE in fluorocarbonates and it is a main component in huttonite and thorite. The detected shift of chemical elements per size fraction because of selective comminution can be caused by different grain sizes, different types of resistance against breakage, or a closer association to other minerals that resist breakage differently.

Quantitative mineralogical analyses conducted in this study using a mineral liberation analyzer show that parisite, synchysite, and bastnaesite respectively constitute approximately 90%, 7%, and 3% of the fluorocarbonates in the South Namxe ore. The non-weighted average of the ratio of $La_2O_3/ThO_2$ is 13.56. For comparison, the ratio of $La_2O_3/ThO_2$ was calculated from literature to be 13.65 based on the average mineral chemistry (Nguyen Thi, 2013) of the South Namxe fluorocarbonates. Owing to some residual uncertainty these ratios are similar to one another; therefore, it is concluded that the fluorocarbonates contain most of the thorium. The available SEM data show that approximately 70% of thorium is bonded to fluorocarbonates and confirm the observations. The quantity of thorium that forms huttonite and thorite and the content of these minerals in the ore are small.

Fig. 11 is a plot of the TREO/F and TREO/CaO ratios. The TREO/F

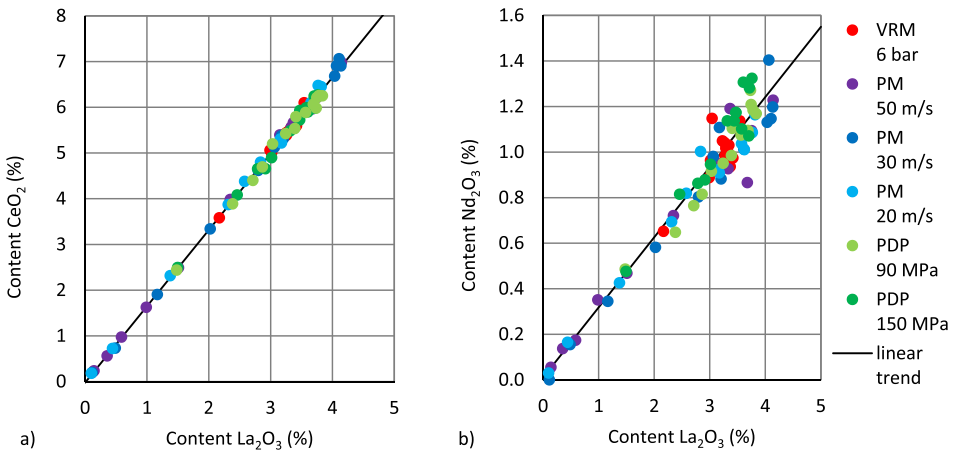


**Fig. 9.** Content of $CeO_2$ (a) and $Nd_2O_3$ (b) versus $La_2O_3$ for all size fractions of all analyzed samples. See Table 1 for abbreviations of machine names and main variable parameters.

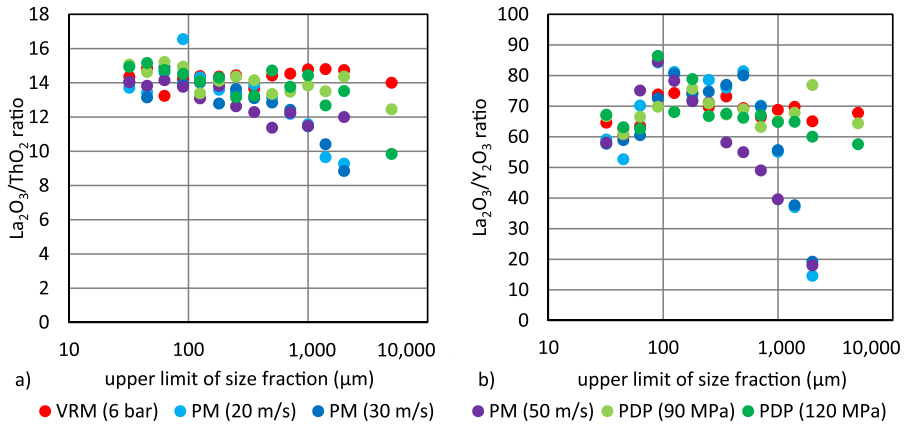


**Fig. 10.** $La_2O_3/ThO_2$ and $La_2O_3/Y_2O_3$ ratios for all analyzed size fractions and comminution products; refer to Table 1 for test abbreviations.

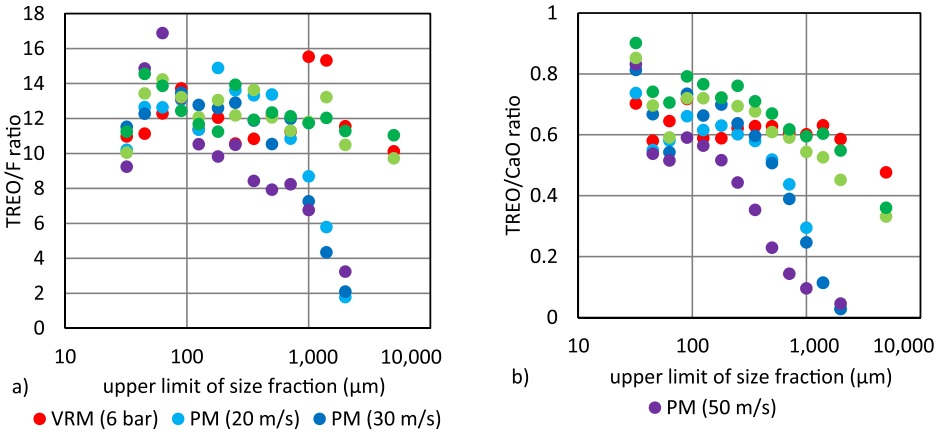


**Fig. 11.** a) TREO/F and b) TREO/CaO ratios for all size fractions and comminution products; refer to Table 1 for test abbreviations.

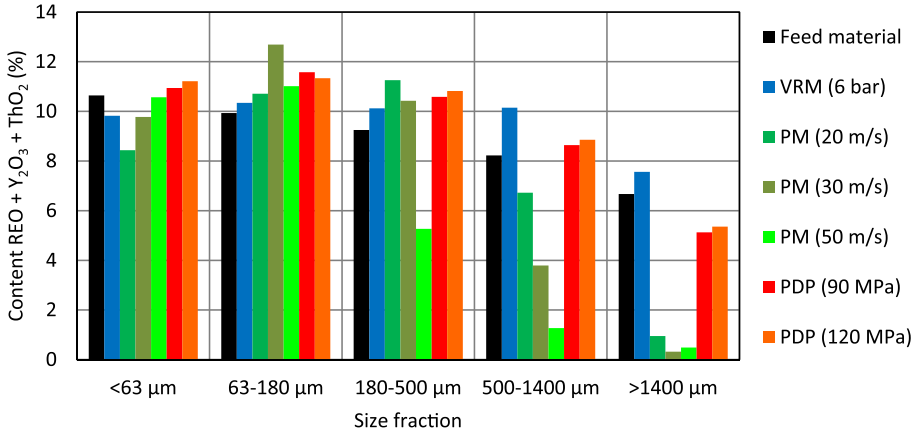


**Fig. 12.** Content of REO + $Y_2O_3$ + $ThO_2$ for different size fractions; for each separate test and feed; refer to Table 1 for test abbreviations.

ratio predominates in the range of 10–14 and the TREO/CaO ratio is mostly in the range 0.4–0.8. Fig. 11 shows a decreasing TREO/CaO ratio with increasing size fraction for tests conducted using the PDP and a significantly steeper decrease for tests conducted using the PM. The CaO content in the samples varies between 11% and 22%. Greater amounts of CaO than REE remain in the coarse fraction. CaO is a main component in some REE minerals (e.g., fluorocarbonates and allanite) and in some barren minerals (e.g., calcite and ankerite). These minerals display a distinctly different behavior during comminution: minerals that contain Ca are distributed to coarse and fine fractions in the comminution products. The shift of fluorocarbonates to the fine fraction is indicated by the enrichment of REEs in the fine fraction. It is assumed that mainly ankerite is responsible for the enrichment of Ca in the large fraction rather than calcite. Ankerite has larger grain sizes and slightly higher hardness (Table 3); therefore, it has a higher probability of remaining in coarser fractions during selective comminution compared to calcite. The depletion of ankerite in the fine fraction and its abundance in coarser fractions is also shown in the mineralogical analyses in Fig. 2 from milling in a ball mill.

Fluorocarbonates and apatite are the only detected minerals with

**Table 3**
Hardness, density, grain sizes and grain shapes (mainly observed) of minerals in the ore veins (red ore); [#2] Cardarelli (2008), [#3] composed from Nguyen Thi et al. (2014), Nguyen Thi (2013), and own measurements.

| Mineral | Calcite | Ankerite | Barite/Celestine/Baryto-celestine | Parisite/Synchysite/Bastnaesite | Apatite |
|---|---|---|---|---|---|
| Mohs Hardness[#2] | 3 [#2] | 3,5–4 [#2] | 3–3,5 [#2] | 4–5 [#2] | 5 [#2] |
| Density[#2] | 2715–2940 [#2] | 2930–3100 [#2] | 4490 [#2] | 4970 (Bastnaesite, [#2]) | 3100–3350 [#2] |
| Grain size[#3] (μm) | 100–300 | 100–2000 | 20–200 | 10–300 | 40–150 (10–200 and clusters up to > 1000 in the rim zone) |
| Grain shape [#3] | euhedral, fractured | anhedral to subhedral | anhedral, fill interstices of fluorocarbonates | Euhedral to subhedral with moderately higher grain roughness | euhedral |

fluorine as a main component (this is supported by electron microprobe investigations not shown here). The correlation between fluorine and the other seven elements (La, Ce, Pr, Nd, Y, Th, Ca see Table 2) ranges from moderate to low. The correlation coefficients take all values into account and do not distinguish between different comminution tests. A more detailed discussion is necessary. The following assumptions are given as reasons for the reduced correlation. The first is that F is distributed to different minerals and the second is that F might be partly substituted by OH groups. The first assumption requires the involvement of different comminution behaviors of fluorocarbonates and apatite, and a different enrichment in size fractions of the comminution products. The second assumption requires an unequal distribution of F and OH to minerals that have different comminution behaviors. This can be extrapolated from existing mineralogical studies; however, it was not included in this study. The ratio between REE and F from the test series using the PM show a significant dependence from the size fraction; the TREO/F ratio decreases with increasing size fraction (Fig. 11a). The TREO content decreases faster than the F content. If the first assumption above is true, it can be concluded that apatite remains in coarser fractions and not fluorocarbonates. Noteworthy is that the grain sizes and hardness of fluorocarbonates and apatite are very similar. Enrichment in the coarser fractions is attributed exclusively to apatite clusters whose sizes range from several millimeters to more than one centimeter. This enrichment may be partially supported by interfacial breakage.

The correlation between REO, $Y_2O_3$, and $ThO_2$ observed above is used to justify summarizing them as TREO + $ThO_2$ in the evaluation below. The size fractions are partly summarized to give concise results. Fig. 12 shows the content of TREO + $ThO_2$ for all analyzed samples, including the distribution of the content of TREO + $ThO_2$ of the feed material. Fine fractions < 500 μm have higher concentrations of TREO + $ThO_2$ than coarse fractions > 500 μm. However, differences in concentrations of TREO + $ThO_2$ for different samples are smaller in the fine fractions and significantly larger in the coarse fractions. The feed material has selectivity, as indicated by the variation in the content of TREO + $ThO_2$ at different size fractions. The gentle sample preparation prior the comminution tests could not fully prevent a remaining selectivity in the test feed material. The TREO + $ThO_2$ content decreases with increasing size fraction, from 10.6% in fractions < 63 μm to 6.7% in fractions > 1400 μm. This trend become stronger in comminution tests conducted using the PDP and PM and become weaker in tests performed in the VRM test rig. Contents of TREO + $ThO_2$ in the size fractions < 1400 μm from the VRM are almost constant (between 9.8% and 10.1%). Approximately 7.6% of TREO + $ThO_2$ are found in the coarsest fraction > 1400 μm. A preferred comminution of barren material is assumed as the cause. The barren material will be enriched in the fine fractions and compensate the pre-existing enrichment of TREO + $ThO_2$ in the feed material.

Products from the PDP test have a content of TREO + $ThO_2$ that is relatively constant (between 10.6% and 11.6%) in fractions < 500 μm, which is slightly above the concentrations of the feed material. Fractions > 1400 μm show significantly low concentrations (5.1% – 5.3%) and are below the concentration of the feed material in the same size fraction. Overall, there are small differences between concentrations of the feed material and products of each size fraction of tests conducted in the PDP.

In contrast, products from the PM reveal a significant depletion of the contents of TREO + $ThO_2$ in the coarse fractions. The fraction > 1400 μm contains 0.3% to 1% of TREO + $ThO_2$. Contents in size fractions of 180/500 μm, 500/1400 μm, and > 1400 μm increase with decreasing size fraction. Concentrations in the fraction < 180 μm approximate those of the fractions of the feed material and products from the VRM and PDP tests. The highest concentrations of each of the PM test materials are reached in the fractions of 63/180 μm and 180/500 μm. Raw data not included in this report show a shift of the highest concentrations to smaller size fractions as impact speed increases. The following concentrations were recorded: 11.8% in the size fraction of 180/250 μm at 20 m/s, 12.8% in the size fraction of 125/180 μm at 30 m/s, and 12.7% in the size fraction of 63/90 μm at 50 m/s. This shift often occurs when selective comminution occurs by impact load. Concentrations of TREO + $ThO_2$ in the fraction < 63 μm of all tests with the PM are below the concentration of the feed material. Barren materials concentrate and dilute the content of TREO + $ThO_2$ from the feed material. It is assumed that there is preferential breakage of barren material and enrichment in the finest fraction.

It is possible that the preferential breakage is superimposed by interfacial breakage of REE minerals. The enrichment of REE minerals in a specific fraction could be attributed to a specific grain size distribution. Interfacial breakage supports enrichment of minerals in size fractions that correspond to their mineral grain size. The petrographic analyses yield grain sizes for the fluorocarbonates that are mainly between 10 μm and 300 μm (Table 3). This corresponds to the observed maximum concentrations in the size fractions of 63–180 μm and 180–500 μm. Further investigations using MLA would be necessary to quantify proportions of interfacial and preferential breakage in the South Namxe ore. A detailed investigation of the grain boundary distribution can prove and quantify the interfacial breakage. Indication from other minerals is that mainly larger (ankerite) or smaller (baryto-celestine) grain sizes are enriched by interfacial breakage in coarser or finer fractions, respectively.

In this study, the SZ Index is calculated for the distribution of the contents of REE minerals and not for elemental concentrations; mineral compositions and distribution were not measured. Several assumptions have to be made when calculating mineral concentrations to achieve simplified mineral compositions and contents. More details could be obtained from measurements of the mineral composition and mineral distribution; however, these were not conducted in the present study. Five assumptions were made. First, only parisite, synchysite, and bastnaesite (all three together are 90% of the REE mineral content, see Fig. 2) were considered. Second, the ideal mineral formulas are used with the exception that all REE, Y, and Th substitute REE on its crystallographic position. Third, the element distributions in the minerals are constant; and fourth, REE, Y, Th were added in a constant ratio to the minerals being considered. Assumption three and four are only valid and are only applied within the size fraction and comminution product one

at a time the corresponding chemical analysis are referring to. Fifth, ratios of these three REE minerals are constant: parisite/synchysite = 12.6 and parisite/bastnaesite = 31.5 (derived from mineralogical analyses). The comminution behavior of these minerals is similar. The MLA analysis confirms an almost constant ratio in the size fraction > 32 µm (see Fig. 2), despite using a different type of comminution: ball mill grinding.

The result of the calculation is mainly affected by high quantities of $La_2O_3$ and $CeO_2$ (in sum 85% of REO + $ThO_2$) in the measured contents of REE + Y + Th and high quantities of parisite. The error from these assumptions is negligible; thus, results of the initial tests are not affected. Furthermore, if the assumptions would not be implemented here, they would be necessary later for interpreting the results. Chemical composition only indicates mineral composition but need a transfer function to quantify the mineral composition as well. Mineralogical analysis support the five assumptions for a transfer function to calculate the mineral content from the chemical element contents. More extensive mineralogical investigations would be necessary to deduce the mineral composition from chemical element measurement and would also show the remaining error if the mineral composition is not measured directly.

Fig. 13 shows the SZ Index of the comminution products and feed material. Selectivity of the feed material is 4%. Selective comminution, mainly preferential breakage, causes changes in selectivity. Selectivity of products from the VRM test rig is below 4%, which yields a negative SZ index. It confirms a reduction in the initial selectivity of the feed material during comminution that was observed in the distribution of the content of TREO + $ThO_2$. Tests conducted in the PM yielded higher values of the SZ index. The highest achieved value is approximately 8.3% at 20 m/s. The SZ index is lower, approximately 6.3% to 6.4% at higher impact velocities of 30 m/s and 50 m/s, respectively. The PDP generates an SZ index of 6.5% at 90 MPa, a value that is similar to the 6.4% achieved at 50 m/s using the PM. The SZ index declines with increasing pressure to reach 6.0% at 120 MPa. The PM and the PDP show well-known trends: selectivity reduces with increasing energy and maximum selectivity is often achieved at low comminution energies. These trends are from initial tests; therefore, have to be used cautiously. The extent of continuation of the increasing trends of the SZ index as the comminution energy decreases is unknown. It is expected that a maximum will be reached at lower comminution energies or that it has already been reached at velocities between 20 m/s and 30 m/s of the PM and pressures of 90 MPa and 120 MPa in the PDP. Influence of many other parameters (e.g., particle size, behavior of the red ore, behavior of the yellow host rock, moisture, and ore: host rock ratio, compression speed, portion of impact and shear load, loading frequency) on selectivity were not investigated.

Conversely, the disadvantage of the SZ index is that the integral value does not provide details of the quality of the concentrate and tailing that can be achieved. Therefore, a recovery plot (Fuerstenau curve in Drzymala, 2006) of the REE minerals and tailing is used (Fig. 14). REE mineral content and non-REE mineral content sum up to 100% for each size fraction and sample. The non-REE mineral content was not measured but calculated as difference from 100% and REE mineral content in each size fraction and sample. The sieve aperture size is the variable parameter that divides a comminution product into a coarse and fine size fraction. If the recovery of barren minerals in the coarse fraction is 100% (top edge in Fig. 14) then the fine fraction is a pure recovery of REE. However, if the recovery of the REE minerals in the fine fraction is 100% (right edge in Fig. 14), then the coarse fraction is a pure recovery of barren material and can be rejected as tailings. The plot of the secondary diagonal represents the line of absolute homogeneous distribution (average value of the whole sample) of valuable and barren materials. Curves for all six analyzed samples are plotted in Fig. 14.

The evaluation focused on the upper left and the lower right corners of Fig. 14. A pure concentrate of REE minerals would plot at the top edge; however, none of the investigated samples represent a high concentrate of REE minerals. Curves that closely approach the secondary diagonal represent samples that contain substantial quantities of barren material and curves that are proximal to the right edge represent pure tailings of barren material. In Fig. 14, recovery curves of products from the PM approach the right edge. This indicates that depleted material from REE minerals can be rejected. For example, 27% of a rejected portion of the barren material in the coarse fraction is equivalent to a recovery of 96.5% of REE minerals in the fine fraction (PM, 20 m/s, 1.4 mm-separation cut). Thereafter, performing a simple calculation, disregarding technical restrictions, includes assuming a similar selectivity in coarser fractions for the same comminution ratio. A beneficiation process has three stages of selective comminution, each with a subsequent sieving process that rejects 27% of the barren material as coarse fraction and loses 3.5% of REE minerals. Finally, 61% (from [100%-(1–0.27)$^3$·100%]) of barren materials can be rejected (>1 mm, if the three-stage comminution starts with a material size of 50 mm and with a comminution ratio of 4 in each stage) with a loss of 10% (from [100%-(1–0.035)$^3$·100%]) of the REE minerals.

## 4. Conclusions

Sensor-based sorting using XRT works exceptionally well on the South Namxe ore in which the main rare earth-bearing mineral is parisite. Performance of our experiment shows that using sensor-based sorting at an early stage of processing can result in mass reduction (to approximately 30%) in the stream. Additionally, our results indicate an enrichment of REE by a factor of 4 in a 1:4 blend of ore to barren material (10/30 mm size fraction) and a loss of less than 2% of rare earth minerals. This could have significant economic benefits if applied in the future development of the deposit. Further tests should be conducted on

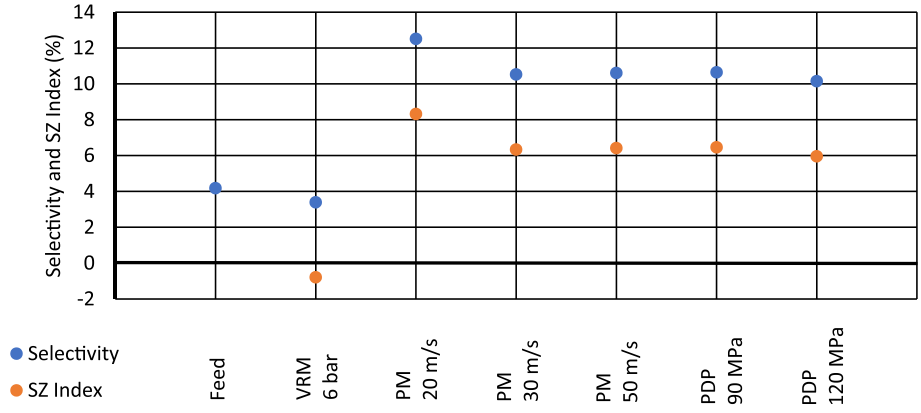


**Fig. 13.** Selectivity and SZ Index for the enrichment of REE minerals; refer to Table 1 for test abbreviations.

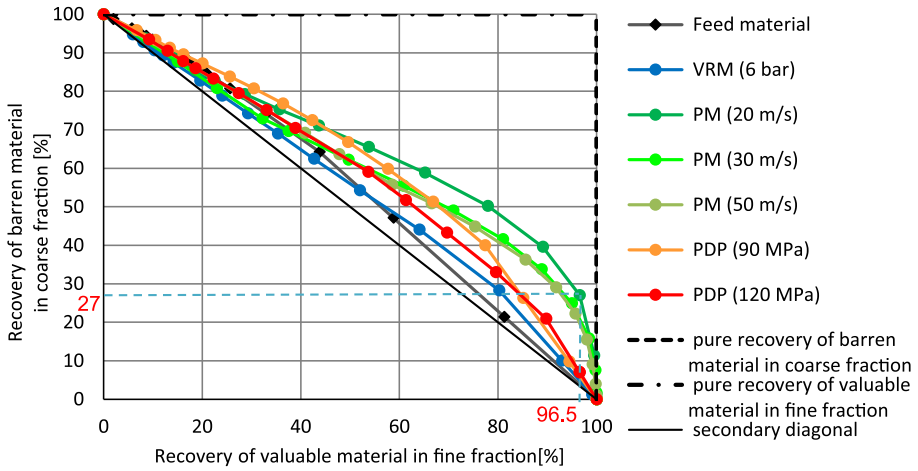


**Fig. 14.** Recovery plot of the course and fine fractions. REE minerals are labeled as valuable and all non-REE minerals as barren material; refer to Table 1 for test abbreviations.

a larger scale to determine the effect of parameters such as the actual host rock/ore ratio according to the mining method, applied comminution techniques, etc., on these results. The MLA data indicated a liberation and selectivity concern evident in the strong mineral association of fluorocarbonates and baryto-celestine with calcite through the different size fractions and liberation classes. This could present a difficulty when processing the ore. To overcome this difficulty, a staged milling or a fractionated flotation process that separately captures coarsely intergrown parisite from coarse to fine fractions can be tested.

Comminution in the confined bed of the PDP resulted in an increase in selectivity from feed to comminution product; the SZ index of the comminution product is slightly higher with low pressure (90 MPa). The PM at velocities of 30 m/s and 50 m/s reaches a similar SZ index to the PDP at a pressure of 90 MPa. The general trend is that low comminution energy results in a higher SZ index. The highest SZ index is reached at 20 m/s. In contrast, the VRM testing rig has a reverse effect on the selectivity of the sampled material and therefore a negative SZ Index. The potential for preferential breakage of the sampled material was not exploited; the existing selectivity of the feed material was reduced, and therefore no REE enrichment could be achieved by sieving. Effect of pressure on the SZ index of samples comminuted in the VRM was not analyzed although it can be assumed low in the investigated pressure range of 4 bars to 8 bars. The three tests conducted in the VRM produced similar particle-size distributions. However, despite similar SZ indexes of tests conducted in the PDP and PM, the products have different qualities after selective comminution. The coarse fractions in the products from the PM have lower REE contents. They can be rejected as tailings. A separation cut of 1.4 mm after a single-stage grinding in the PM at 20 m/s rejects 27% of the barren material and significantly low quantities of REE (3.5%). This result is close to the result of XRT sorting. The coarse fractions in the products from the PDP tests have higher REE contents. Rejection of these fractions would result in higher losses. The fine fractions of all products contain significant quantities of barren material and need further processing to obtain concentrates of REE.

Several other important influencing parameters were not considered in this investigation. It is necessary to examine different particle sizes and the comminution behavior of the red ore and the other host rocks. A more detailed measurement of structure and texture (e.g., grain size and grain shape distribution) and a measurement of the general mechanical properties of minerals in the red ore and host rocks are necessary to describe the potential for selective comminution. Selective comminution can be applied to different separation requirements, including separation of ore veins from host rock or separation of ore minerals from barren minerals, which requires a quantitative material description for any given particle size. Further investigation on selective comminution with focus on interfacial breakage could be utilized to address the challenge to liberate parisite from baryto-celestine. Compression loads in both vertical roller mills and high-pressure grinding rolls are known to facilitate interfacial breakage. This phenomenon was not evaluated or quantified in this study. However, the distribution of the REO content in the size fractions similar to the fluorocarbonates grain size indicates a possible occurrence of interfacial breakage. The effect of selective comminution, regardless of the influence of interfacial or preferential breakage on flotation, should be further investigated.

In industrial application, selective comminution is performed in multi-stage comminution. Comminution at different particle sizes typically requires the use of different machines or different parameter settings. Our experiment is considered as a first approach and further investigations are required to establish a processing strategy. Pretreatment of samples using electrodynamic pulses is known to have an additional positive effect on the degree of liberation during selective comminution. However, sensor-based sorting is limited by the challenge of applicable particle sizes and depends on pre-comminution processes, resulting in adequate quantities of suitable size fractions to enter the sensor sorting process. Selective comminution can handle a much larger range of feed particle sizes— from some hundred millimeters down to below one millimeter. The upper limit is mostly defined by the potential for selective comminution and machine properties. The earliest stage for applying selective comminution is blasting. It is not investigated yet if blasting can cause a distinct particle size difference between REE containing carbonatite veins and barren host rock. Pre-crushing with gyratory crusher or jaw crusher hardly support preferential breakage. The comminution principal in both machines is not sensitive enough to different rock compressive strength. Impact crusher are much more sensitive to different rock compressive strength but are limited by feed particle size and compressive strength of the host rock. The lower limit is typically given by the possibility to use the exploited potential— for example, by sieving or flotation. Finally, selective comminution can additionally be applied to relevant quantities of undersize middle fraction produced from pre-comminution for sensor-based sorting. Nonetheless, it should be considered that larger quantities of the material with the highest potential for preferential breakage have undergone sensor-based sorting. Understanding the relationship between preferential breakage and sensor-based sorting in a combined application requires further investigations. Furthermore, it should be emphasized that this study contains preliminary tests, undertaken with highest care with a limited amount of sample material and is supposed to serve as a basis for further, more detailed investigation.

## CRediT authorship contribution statement

**Alan Cardenas-Vera:** Conceptualization, Investigation, Writing – original draft. **Max Hesse:** Conceptualization, Investigation, Writing – original draft. **Robert Möckel:** Funding acquisition, Conceptualization, Investigation, Writing – review & editing. **R. Gerhard Merker:** Methodology, Investigation. **Thomas Heinig:** Investigation. **Quang Van Phan:** Resources, Funding acquisition.

## Declaration of Competing Interest

The authors declare that they have no known competing financial interests or personal relationships that could have appeared to influence the work reported in this paper.

## Acknowledgments

Alan Cardenas-Vera wishes to acknowledge the study fellowship under the ERASMUS-MUNDUS International Master Program in Resources Engineering—EMERALD. The authors would like to thank the Vietnamese Ministry of Science and Technology (MOST, Code NDT.02. GER/15) and the German Federal Ministry of Education and Research (BMBF, grant number: BMBF 033R120B) for funding this international research project (REE Namxe). Furthermore, we thank the Hung Hai Group for providing access to exploration drill cores and Doreen Ebert for helping with sample handling and analytical assistance. The authors would also like to thank two anonymous reviewers who helped to improve the quality of the manuscript.

## References

Bachmann, K., Frenzel, M., Krause, J., Gutzmer, J., 2017. Advanced Identification and Quantification of In-Bearing Minerals by Scanning Electron Microscope-Based Image Analysis. Microsc. Microanal. 23 (3), 527–537. https://doi.org/10.1017/S1431927617000460.

Cardarelli, F., 2008. Materials Handbook: A Concise Desktop Reference, 2, Edition. ed. Springer International Publishing, London.

Drzymala, J., 2006. Atlas of upgrading curves used in separation and mineral science and technology. Part I Physico-Chem. Problems Mineral Process. 40, 19–29.

Dzien, D.V., 1990. Rare Earth Deposits, in: Geology and Mineral Resources of Vietnam. pp. 144–147.

Fandrich, R., Gu, Y., Burrows, D., Moeller, K., 2007. Modern SEM-based mineral liberation analysis. Int. J. Miner. Process. 84 (1-4), 310–320. https://doi.org/10.1016/j.minpro.2006.07.018.

Hanor, J.S., 2000. Barite-celestine geochemistry and environments of formation. Rev. Mineral. Geochemistry 40, 193–275. https://doi.org/10.2138/rmg.2000.40.4.

Heinig, T., Bachmann, K., Tolosana-Delgado, R., Van Den Boogaart, G., Gutzmer, J., 2015. In: Monitoring gravitational and particle shape settling effects on MLA sampling preparation. International Association for Mathematical Geosciences, Freiberg, pp. 200–206.

Heinig, T., Möckel, R., Krause, J., Gutzmer, J., Quang, V.P., Burisch, M., 2019. Magmatic vs hydrothermal - origin of parisite-hosted REE mineralization at Nam Xe. In: Proceedings of the 15th SGA Biennial Meeting, pp. 1740–1743.

Hesse, M., 2018. Selektive Zerkleinerung von Erzen und Industriemineralen bei Prallbeanspruchung (Selective comminution of ores and industrial minerals at impact load). Technische Universität Bergakademie Freiberg.

Hesse, M., Popov, O., Lieberwirth, H., 2017. Increasing efficiency by selective comminution. Miner. Eng. 103–104, 112–126. https://doi.org/10.1016/j.mineng.2016.09.003.

Kušnír, I., 2000. Mineral resources of Vietnam. Acta Montan. Slovaca 5, 165–172.

Lessard, J., De Bakker, J., McHugh, L., 2014. Development of ore sorting and its impact on mineral processing economics. Miner. Eng. 65, 88–97. https://doi.org/10.1016/j.mineng.2014.05.019.

Lessard, J., Sweetser, W., Bartram, K., Figueroa, J., McHugh, L., 2016. Bridging the gap: Understanding the economic impact of ore sorting on a mineral processing circuit. Miner. Eng. 91, 92–99. https://doi.org/10.1016/j.mineng.2015.08.019.

Long, K.R., Van Gosen, B.S., Foley, N.K., Cordier, D., 2012. The Principal Rare Earth Elements Deposits of the United States: A Summary of Domestic Deposits and a Global Perspective. In: Sinding-Larsen, R., Wellmer, F.-W. (Eds.), Non-Renewable Resource Issues. Springer Netherlands, Dordrecht, pp. 131–155. https://doi.org/10.1007/978-90-481-8679-2_7.

Merker, G., Heinig, T., Balinski, A., Quang, V., Möckel, R., 2019. Parisite flotation from carbonatite REE-ore. In: Proceedings of the 9th International Flotation Conference. Cape Town, pp. 1103–1119.

Möckel, R., Heinig, T., Cardenas-Vera, A., Gutzmer, J., Merker, G., Quang, V., 2019. Beneficiation of parisite-rich rare earth ore from the Nam Xe South deposit, Vietnam. In: Proceedings of the 15th SGA Biennial Meeting, pp. 1508–1511.

Neubert, K., Wotruba, H., 2017. Investigations on the Detectability of Rare-Earth Minerals Using Dual-Energy X-ray Transmission Sorting. J. Sustain. Metall. 3 (1), 3–12. https://doi.org/10.1007/s40831-016-0069-1.

Nguyen Thi, T., 2013. Study on geochemistry of the South Nam Xe carbonatites, northwest Vietnam. Shizuoka University.

Nguyen Thi, T., Wada, H., Ishikawa, T., Shimano, T., 2014. Geochemistry and petrogenesis of carbonatites from South Nam Xe, Lai Chau area, northwest Vietnam. Mineral. Petrol. 108, 371–390. https://doi.org/10.1007/s00710-013-0301-7.

Owens, C.L., Nash, G.R., Hadler, K., Fitzpatrick, R.S., Anderson, C.G., Wall, F., 2018. Zeta potentials of the rare earth element fluorcarbonate minerals focusing on bastnäsite and parisite. Adv. Colloid Interface Sci. 256, 152–162. https://doi.org/10.1016/j.cis.2018.04.009.

Phan, Q.V., Dao, T.T., Nguyen, P., Trinh, D.H., Heinig, T., 2019. An assessment of natural radioactivity in the namxe rare earth deposit, Laichau province, Vietnam. Minerals 9, 1–12. https://doi.org/10.3390/min9100602.

Robben, C., Wotruba, H., 2019. Sensor-based ore sorting technology in mining—past, present and future. Minerals 9, 1–25. https://doi.org/10.3390/min9090523.

Schulz, B., Merker, G., Gutzmer, J., 2019. Automated SEM mineral liberation analysis (MLA) with generically labelled EDX spectra in the mineral processing of rare earth element ores. Minerals 9 (9), 527. https://doi.org/10.3390/min9090527.

Smith, M.P., Moore, K., Kavecsánszki, D., Finch, A.A., Kynicky, J., Wall, F., 2016. From mantle to critical zone: A review of large and giant sized deposits of the rare earth elements. Geosci. Front. 7 (3), 315–334. https://doi.org/10.1016/j.gsf.2015.12.006.

Veras, M.M., Young, A.S., Born, C.R., Szewczuk, A., Bastos Neto, A.C., Petter, C.O., Sampaio, C.H., 2020. Affinity of dual energy X-ray transmission sensors on minerals bearing heavy rare earth elements. Miner. Eng. 147, 106151. https://doi.org/10.1016/j.mineng.2019.106151.

Vlasov, I., Efremov, I., Son, N.C., Doc, N., A, H., 1961. Concluded report of exploring project on Nam Xe rare earth - ore deposit (1958 - 1960 stage).

Wotruba, H., Harbeck, H., 2010. Sensor-Based Sorting, Ullmann's Encyclopedia of Industrial. Chemistry. 395–404. https://doi.org/10.1002/14356007.b02_18.pub2.

Zhou, B., Li, Z., Chen, C., 2017. Global potential of rare earth resources and rare earth demand from clean technologies. Minerals 7 (11), 203. https://doi.org/10.3390/min7110203.